Supporting Information

Evaluating Early Apoptosis-Related Cellular MiRNAs with an Ultrasensitive Electrochemiluminescence Nanoplatform

Haiying Cai[a], Peiting Dong[a], Xiuping Li[a], Lulu Wang[a], Lili Shi[b]* and Tao Li[a]*

[a] Department of Chemistry, University of Science and Technology of China, 96 Jinzhai Road, Hefei, Anhui 230026, China. E-mail: tlitao@ustc.edu.cn

[b] Department of Chemistry, Anhui University, 111 Jiulong Road, Hefei, Anhui 230601, China. E-mail: llshi@ustc.edu.cn.

Table of Contents
Supplementary Figures

Supplementary Table
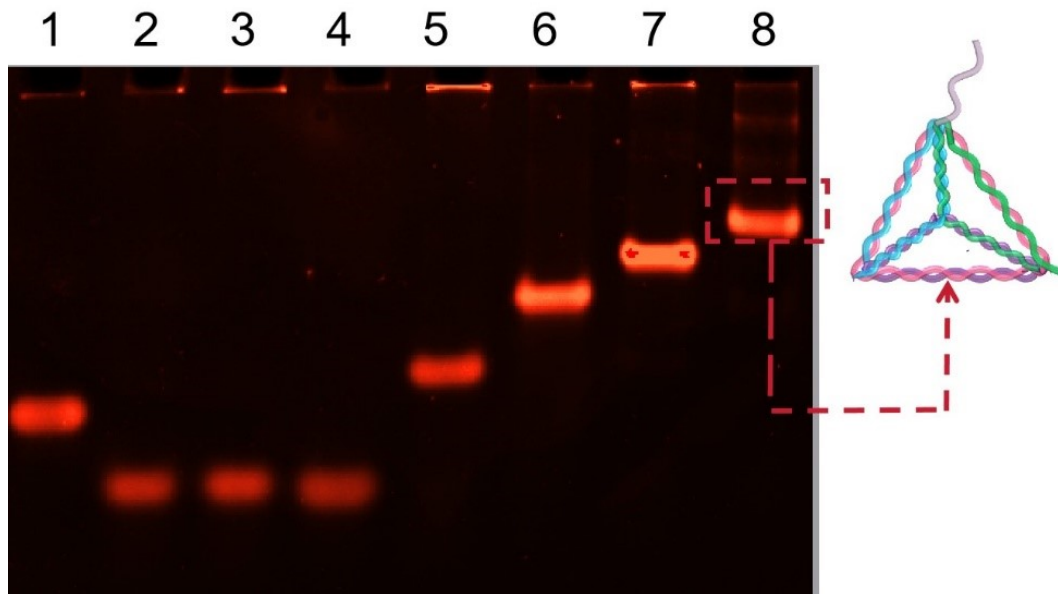
Supplementary Figures

Fig. S1. PAGE analysis of TDNs: lane 1, S1; lane 2, SH-S2; lane 3, SH-S3; lane 4, SH-S4; lane 5, S2+S3; lane 6, S2+S3+S4; and lane 7, S1+S2+S3+S4 (TDNs). TDN nanostructures were assembled by four DNA single strands, where there are three thiolated strands anchored on the electrode surface and a capture strand associated with probe and target. To verify the formation of TDNs, PAGE was conducted. As shown in Fig.S3, only do four strands mix together, the lane 7 emerges slowest migration which demonstrates the successful synthesis of TDNs.
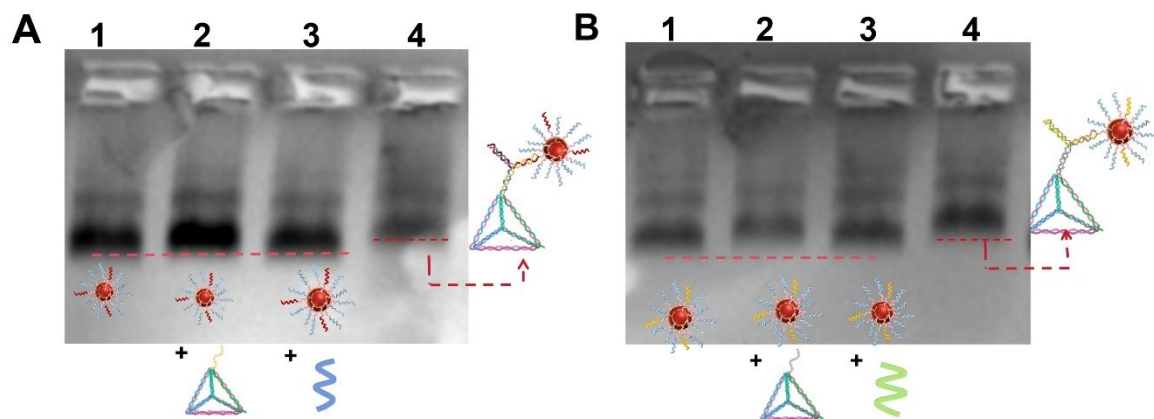
Fig. S2. AGE analysis of Y-shaped construction. (A): lane 1, SNAzyme; lane 2, SNAzyme and TDNs; lane 3, SNAzyme and miR-21; lane 4, SNAzyme, miR-21 and TDNs. (B): lane 1, SNAzyme; lane 2, SNAzyme and TDNs; lane 3, SNAzyme and miR-133a; lane 4, SNAzyme, miR-133a and TDNs; AGE gel electrophoresis verifies that the Probe chain can assemble Y-shaped structure on AuNPs surface by interaction with the Capture chain on tetrahedron in the presence of target chain. Band displacement in AGE electrophoresis is only related to molecular weight. As shown in Fig.S3 A (target chain miR-21) and S3B (target chain miR-133a), the strip positions displayed in channel 2 and 3 are basically consistent with the strip positions of channel 1, only the strip of channel 4 is obviously above the other three channels. The results showed that the DNA migration rate in channel 4 was slower than that in the other three channels, indicating that when only the target chain existed, TDN and SNA assembled to form a Y-shaped structure, and the molecular weight was the highest at this time, which provided the basis for subsequent assembly of the Y-shaped structure on the electrode surface.
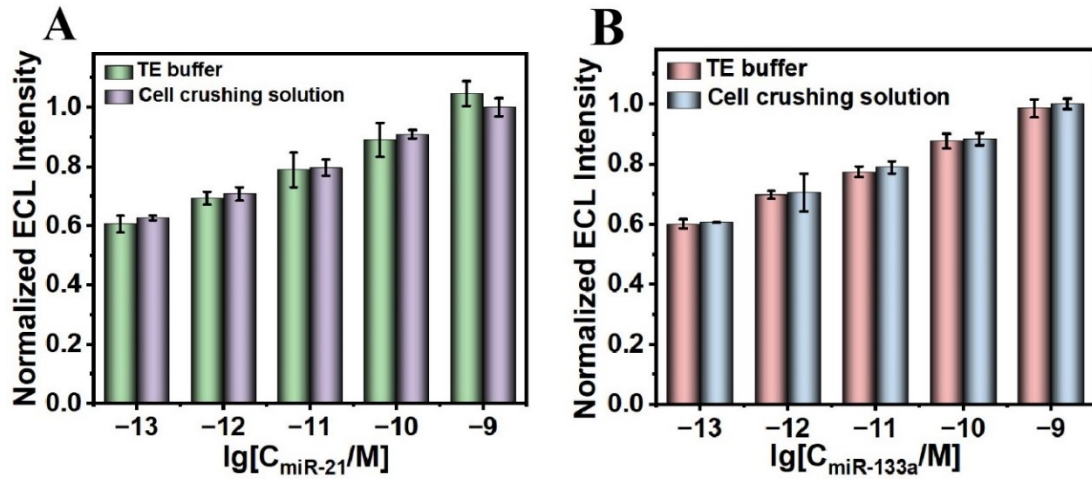
Fig. S3. miR-21 (A) and miR-133a (B) ECL performance of the designed biosensor in 10^5 cells/ml crushing solution. Comparison of ECL intensity toward different concentrations of miR-21 and miR-133a in TE buffer and cell crushing solution.
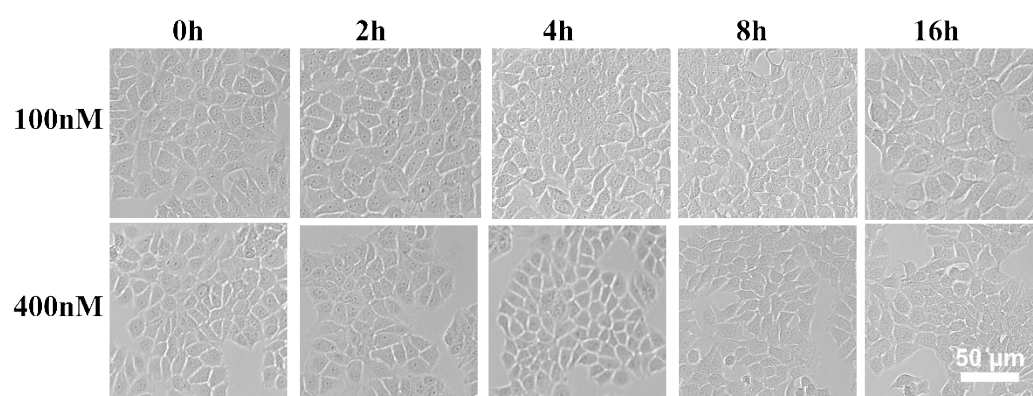
Fig. S4. The morphological changes of MCF-7 cells before and after DOX treatment at 100nM and 400nM, DOX action time gradients were 0、2、4、8、16h.

Supplementary Table

Table S1. DNA and microRNA sequences about this work

DNA Name	DNA sequence (5'-3')
A5T30-PW17C	AAA AAT TTT TTT TTT TTT TTT TTT TTT TTT TTT TTG GGT AGG GCG GGT TGG GTC
A5T30-Y2-12	AAA AAT TTT TTT TTT TTT TTT TTT TTT TTT TTT CAA CAT CAG TCC AGT AAC AGC G
A5T30-Y2	AAA AAT TTT TTT TTT TTT TTT TTT TTT TTT TTT TTA AAC ATC ACT CAG TAA CAC GC
A5T30-Y2-208a	AAA AAT TTT TTT TTT TTT TTT TTT TTT TTT TTT TTA CAA GCT TTT CAG TAA CAC GC
A5T30-Y2-13a	AAA AAT TTT TTT TTT TTT TTT TTT TTT TTT TTT TTC AGC TGG TTG ACA GTA ACA CGC
TDN-S1	ACA TTC CGT CTG AAA CAT TAC ATG CTA CAC GAG AAG AGC CAT AGT ATT TTT TTT TTC CGT GTT ACT GGC AAG TCT TAA
S1-133a	ACA TTC CGT CTG AAA CAT TAC ATG CTA CAC GAG AAG AGC CAT AGT ATT TTT TTT TTC CGT GTT ACT GAG GGG ACC AAA
S1-208a	ACA TTC CGT CTG AAA CAT TAC ATG CTA CAC GAG AAG AGC CAT AGT ATT TTT TTT TTC CGT GTT ACT GTG CTC GTC TTA T
S1-21-8	ACA TTC CGT CTG AAA CAT TAC ATG CTA CAC GAG AAG AGC CAT AGT ATT TTT TTT TTT GTT ACT GTG ATA AGC TA
TDN-S2	TTC AGA CGG AAT GTG CTT CCC AAG TGT CGT AAG TAT TGG CTC GCA T
TDN-S3	TCA ACT GGG TGA TAA AAC GAC ACT TGG GAA TCT ACT ATG GCT CTT C
TDN-S4	TTC AGA CGG AAT GTG CTT CCC AAG TGT CGT AAG TAT TGG CTC GCA T
miR-21	UAG CUU AUC AGA CUG AUG UUG A
miR-133a	UUU GGU CCC CUU CAA CCA GCU G
miR-499	UUA AGA CUU GCA GUG AUG UUU
miR-208a	AUA AUA CGA GCA AAA GCU UGU
miR-16	UAG CAG CAC GTA A AT ATT GGC G
miR-328	CUG GCC CUC UCU GCC CUU CCG U

Table S2. Comparison of the miR-21 and miR-133a detection performance between the proposed strategy and other biosensors.

Method	Target	Linear range	LOD	References
CL	miR-21	5 fM~10 nM	1 fM	[1]
CL	miR-21	10 fM~10 nM	8.32 fM	[2]
FL	miR-21	2.5 fM~1 nM	161 fM	[3]
FL	miR-21	50 fM~1 pM	1.3 fM	[4]
ECL	miR-21	100 fM~100 nM	30.2 fM	[5]
ECL	miR-21	100 aM~10 pM	61.7 aM	[6]
ECL	miR-21	100 aM~1nM	33 aM	This work
CL	miR-133a	10 pM~100nM	0.3 pM	[7]
CL	miR-133a	10 fM~100nM	0.2 fM	[8]
FL	miR-133a	100 fM~10nM	74.9 fM	[9]
FL	miR-133a	0.1 nM~20nM	40 pM	[10]
ECL	miR-133a	1 fM~1nM	0.33 fM	[11]
ECL	miR-133a	0.1 fM~1nM	66.2 aM	[12]
ECL	miR-133a	100 aM~1nM	33 aM	This work

Reference

[1] He C, Chen S, Zhao J, Tian J, Zhao S.Talanta, 2020, 209: 120505.

[2] Zhao S, Jia Y, Wang A, Yang J, Yang L. Biosens Bioelectron., 2023, 239: 115613.

[3] Zhe Lu, Wei Ni, Nian Liu, Dan Jin, Tingxian Li, Kun Li, Yuling Zhang, Qunfeng Yao, Guo-Jun Zhang. Microchem J., 2023, 187: 108370.

[4] Huang Q, Wang K, Wang Y. Talanta, 2024, 273: 125928.

[5] Ma C, Zhou Q, Shi J, Gao H, Huang D, Xue H, Wang H, Zhang Z, Yang S, Zhang J, Zhang K.Talanta, 2024, 266: 125125.

[6] Wang X, Wang X, Hu C, Guo W, Wu X, Chen G, Dai W, Zhen S, Huang C, Li Y. Biosens Bioelectron. 2022, 213: 114443.

[7] Sun Y, Shi L, Wang Q, Mi L, Li T. Anal Chem., 2019, 91(5): 3652-3658.

[8] Shi L, Sun Y, Mi L, Li T. ACS Sensors, 2019, 4(12): 3219-3226.

[9] Chen L, Li ZY, Zhang J, Zhao Y, Hu R, Yang YH, Yang T .Talanta, 2024, 266: 125032.

[10] Cheng X, Ren D, Xu G, Wei F, Yang J, Xu J, Wang L, Hu Q, Cen Y. Biosens Bioelectron., 2022, 196: 113706.

[11] Yu L, Zhu L, Yan M, Feng S, Huang J, Yang X. Anal Chem., 2021, 93(34): 11809-11815.

[12] Zong C, Kong L, Li C, Xv H, Lv M, Chen X, Li C. Mikrochim Acta., 2024, 191(4): 223.